



Water gas shift reaction over multi-component ceria catalysts

Vijay M. Shinde, Giridhar Madras*

Department of Chemical Engineering, Indian Institute of Science, Bangalore 560 012, India

ARTICLE INFO

Article history:

Received 14 February 2012

Received in revised form 2 May 2012

Accepted 3 May 2012

Available online 14 May 2012

Keywords:

Water gas shift

Ceria supported catalyst

Oxygen storage capacity

Reaction mechanism

ABSTRACT

This study reports the activity of ionic substituted bimetallic Cu-Ni-modified ceria and Cu-Fe-modified ceria catalysts for low-temperature water gas shift (WGS) reaction. The catalysts were synthesized in nano-crystalline size by a sonochemical method and characterized by XRD, TEM, XPS, TPR and BET surface analyzer techniques. Due to the ionic substitution of these aliovalent base metals, lattice oxygen in CeO_2 is activated and these catalysts show high activity for WGS at low temperature. An increase in the reducibility and oxygen storage capacity of bimetallic substituted CeO_2 , as evidenced by H_2 -TPR experiments, is the primary reason for the higher activity towards WGS reaction. In the absence of feed CO_2 and H_2 , 100% conversion of CO with 100% H_2 selectivity was observed at 320 °C and 380 °C, for Cu-Ni-modified ceria and Cu-Fe-modified ceria catalysts. Notably, in the presence of feed H_2O , a reverse WGS reaction does not occur over these ceria modified catalysts. A redox reaction mechanism, involving oxidation of CO adsorbed on the metal was developed to correlate the experimental data and determine kinetic parameters.

© 2012 Elsevier B.V. All rights reserved.

1. Introduction

Fuel cell technology is an attractive, energy efficient process for both power plant and transportation applications. However, before realizing any benefit from the fuel cell, hydrogen with sufficient purity must be generated [1]. The reformat gas is the main source of H_2 , which contains about 8–10% CO. The high levels of CO produced in the reformat demonstrate the need for WGS catalysts, as CO can be converted to CO_2 by reaction with H_2O , with the added advantage of generating more H_2 . This high level of CO is mitigated to about 3–5% by high-temperature water-gas shift (HTS) run at near equilibrium conditions [2]. The low-temperature water-gas shift (LTS) can be used in tandem with HTS step to achieve even higher CO conversions. However, CO needs to be removed below 50 ppm upstream of a polymer-electrolyte fuel cell (PEFC), because it poisons the membranes and the noble metal catalysts of fuel cell [3,4]. Thus, WGS reaction constitutes an integral part of fuel cell power system. Reducing the size of the WGS reactor is important from an economical point of view and the development of an efficient and stable WGS catalyst is highly desirable for the integration of the reformer with the fuel cell. In addition to this, the high WGS activity at low temperature is crucial because it would allow the reaction to be carried out at lower temperatures where the reaction is mainly driven by kinetics and not by the thermodynamics.

For large scale applications, the WGS reaction is typically conducted over commercial catalysts based on iron or copper. However, for mobile applications, these conventional catalysts are not ideal because of their sensitivity to start-up/shut-down cycles, and pyrophoricity in case of Cu based catalysts [5]. Further, lengthy and difficult reduction procedures associated with these commercial catalysts are also prohibitive and not acceptable in fuel cell applications [6]. Ceria promoted/supported metals, such as Pt, Rh, Pd, Ni, Cu, and Fe seems to be promising candidates and are receiving widespread attention as good LTS catalysts [7–10]. It has also been reported that Au supported on reducible oxides such as CeO_2 , TiO_2 , Fe_2O_3 , etc., shows a remarkably high activity for the WGS reaction [11–13]. However, gold based catalysts are very sensitive to preparation conditions [14] and requires a large metal loading (~5%), which makes them prohibitively expensive for large-scale applications [9]. WGS has also been studied on Pt, Pd and Au supported catalysts involving CeO_2 , ZrO_2 and CeO_2 - ZrO_2 by several investigators [15–17].

Ceria is a key component of three way catalysts in automotive exhaust, because of its oxygen storage capacity (OSC) [18,19]. The facile $\text{Ce}^{4+} \leftrightarrow \text{Ce}^{3+}$ redox shuttle is demonstrated to be the driving force for this behavior. The utilization of lattice oxygen via the exchange process $2\text{CeO}_2 \leftrightarrow \text{Ce}_2\text{O}_3 + 1/2\text{O}_2$ has been conceived under reducing conditions. However, the role of ceria as a carrier of a metal supported catalyst is not only related to its high OSC but also to the improved dispersion of the metal [7,20]. Metal-ceria systems are several orders of magnitude more active than metal/alumina for a number of redox reactions including WGS reaction [21,22]. The oxygen vacancy in the ceria supported catalysts alters the

* Corresponding author. Tel.: +91 80 22932321; fax: +91 80 23601310.

E-mail addresses: giridhar@chemeng.iisc.ernet.in, giridharmadras@gmail.com (G. Madras).

morphology and dispersion of the supported metal [23,24]. Metal-modified ceria has a higher oxygen storage capacity (OSC) and reducibility than pure ceria [25]. Metal supported ceria acts as a bi-functional catalyst in which CO is adsorbed on the metal sites and H₂O dissociation take place on the oxide vacancy leading to higher activity. This has been investigated thoroughly recently [3,21,26–28]. Therefore, it is of interest to explore the LTS catalyst based on the ceria materials.

The Cu-and other transition metal-containing nanocrystalline ceria supports are active and stable catalysts in low and high-temperature WGS reactions [10,29]. The reducibility and WGS activity of CeO₂ are significantly enhanced by the presence of a small amount of a transition metal, which it has not necessarily to be a Pt group metal [30]. The effectiveness of other cheap base metals in comparison with Pt, Pd in promoting the reduction of ceria needs to be explored.

We have previously reported the catalytic activity of noble metal substituted CeO₂ and CeO₂-ZrO₂ solid solution for WGS reaction [8]. However, the use of bimetallic base metal ion substitution for Ce⁴⁺ for WGS reaction has not been reported in the literature. In this work, we have studied the WGS reaction over both Cu-Ni and Cu-Fe-modified CeO₂ catalysts to further elucidate the properties of these ceria-based materials towards WGS. The catalysts were synthesized by a sonochemical method and characterized by various techniques. The effect of ionic substitution of the base metals on the reducibility of ceria was determined by temperature programmed reduction (H₂-TPR) method and their OSC was compared at various temperatures. The spectroscopic insights and the various experimental observations were used to derive the kinetic expressions for WGS over these catalysts.

2. Experimental

2.1. Catalysts preparation and characterization

Ce_{0.75}Cu_{0.1}Ni_{0.15}O_{2-δ} and Ce_{0.7}Cu_{0.1}Fe_{0.2}O_{2-δ} were prepared by the sonochemical method. Chemical reagents including ammonium cerium (IV) nitrate (CAN) [(NH₄)₂Ce(NO₃)₆], Nice Chemicals, India), copper nitrate ([Cu(NO₃)₂·3H₂O], S.D Fine, India), ferric nitrate ([Fe(NO₃)₃·9H₂O], S.D Fine, India), nickel nitrate ([Ni(NO₃)₂·6H₂O], S.D Fine, India), diethylenetriamine (DETA) [C₄H₁₃N₃] S.D Fine, India) were used as received without further purification. In the sonochemical method, (NH₄)₂Ce(NO₃)₆, Cu(NO₃)₂·3H₂O, and Ni(NO₃)₂·6H₂O were taken in the molar ratio of 0.75:0.1:0.15 to synthesize Ce_{0.75}Cu_{0.1}Ni_{0.15}O_{2-δ}. 5 g of CAN, 0.3 g of copper nitrate, 0.53 g of nickel nitrate were dissolved in 100 ml of distilled water under vigorous stirring until a homogeneous solution was obtained. 5 ml of DETA was then added to the solution and the solution turned immediately into a gel. The gel was ultrasonically irradiated under ambient conditions with a high-intensity ultrasonic probe (125 W) immersed directly in the solution for 5 h. During sonication, the temperature of the solution reached up to 60 °C. At the end of reaction time, the mixture was centrifuged and washed with deionized water and absolute ethanol and dried in a hot air oven at 120 °C for 2 h. A similar procedure was followed for the synthesis of Ce_{0.7}Cu_{0.1}Fe_{0.2}O_{2-δ}. Both catalysts were used in all catalytic studies without any pretreatment. Base metal impregnated on a CeO₂ catalyst was also prepared by reducing the respective metal nitrate solution by hydrazine hydrate (99%, S.D Fine, India) over CeO₂ made by the sonochemical method. The solution was filtered and dried at 120 °C for 3 h. The resulting dried solid was further reduced in 5% H₂ balance with argon at 250 °C for 30 min before the catalytic activity test.

Powder diffractograms on catalysts were recorded using a Philips X'Pert diffractometer using high-intensity Cu Kα (40 kV,

30 mA) radiation. A secondary beam graphite monochromator in the 2θ range of 20–80° at 0.02° min⁻¹ was used for measurement. The program suite JANA 2000 was used to perform profile fitting, lattice parameter refinement and microstructure analysis. The sizes, morphologies and state of agglomeration of the synthesized catalysts were observed by transmission electron microscopy (TEM) using a FEI Technai 20 electron microscope operating at 200 kV. TEM samples were prepared by suspending the dried catalyst in ethanol with a sonication bath for 10 min. A drop of the sample suspension was allowed to dry on a copper grid (300 mesh) coated with a carbon film. A Thermo Scientific Multilab 2000 X-ray Photoelectron Spectrometer with a resolution of 0.1 eV was used to determine the metal oxidation state of selected catalysts. An Al Kα X-ray source was used in this work. All binding energies were adjusted to the C 1s peaks at 285 eV. BET surface area measurements were made with a Quantachrome NOVA 1000 gas adsorption analyzer.

2.2. Temperature-programmed reduction (H₂-TPR)

H₂-TPR was used to study the influence of ionic substitution of base metals on ceria reducibility. Redox properties or OSC of both the catalysts were studied by H₂-TPR or hydrogen uptake. There is direct relation between oxygen storage capacity (OSC) and activity of catalyst. The reduction/oxidation processes on the catalyst surface were examined by performing H₂-TPR studies. Catalyst samples were prepared by pressing thin disks from powders and breaking the disks into small granules of 50–100 mesh sizes and loaded in the quartz reactor of 40 cm length and 0.4 cm of internal diameter. The degree of reduction measurements as a function of temperature were carried out over 50 mg of catalyst in a reactor with 5% H₂/Ar (Chemix, Bangalore, India) flowing at 30 ml/min. The temperature of reactor was increased from 35 to 600 °C at a ramp rate of 10 °C min⁻¹. A moisture trap was used to capture any water desorbed from the catalyst prior to entering the TCD. The hydrogen was purged with a flow of argon prior to the oxidation of catalyst. The amount of H₂ consumption or equivalent [O] release was determined from hydrogen intake/consumption of a known weight of CuO sample.

2.3. Catalytic activity test

The activity of the both catalysts towards the WGS reaction, expressed as the degree of CO conversion, was evaluated over a wide range of temperature (120–380 °C). The activity for WGS was measured in a quartz tubular reactor (0.4 cm ID) using 300 mg of catalyst, which was heated inside an electric furnace. The temperature of furnace was controlled by PID controller. The catalyst sample was diluted with glass beads of 50–100 mesh sizes and the corresponding gas hour space velocity was (GHSV on the dry basis) 48,000 h⁻¹. All catalysts were used in the as-prepared form without further activation. Activation was only applied to impregnated catalysts used in the activity tests for comparison with the bimetallic ionic-ceria catalysts. All experiments were measured at 1 atm total pressure with the partial pressures controlled by the relative flow rates. The feed gas mixture was used that consists of 2 vol% CO with balance of N₂ such that total gas flow rate was 100 ml/min. Water was injected into the flowing gas stream by a calibrated HPLC pump and vaporized in the heated gas feed line before entering the reactor. The flow rate of water vapor was maintained at 55 ml/min for all experiments and was found to be sufficient to achieve the highest CO conversion. A condenser filled with ice was installed at the reactor exit to collect water. The reaction was carried out at isothermally at several temperatures.

The concentration of the effluent from the reactor was determined using an on-line gas chromatograph (Mayura Analytical,

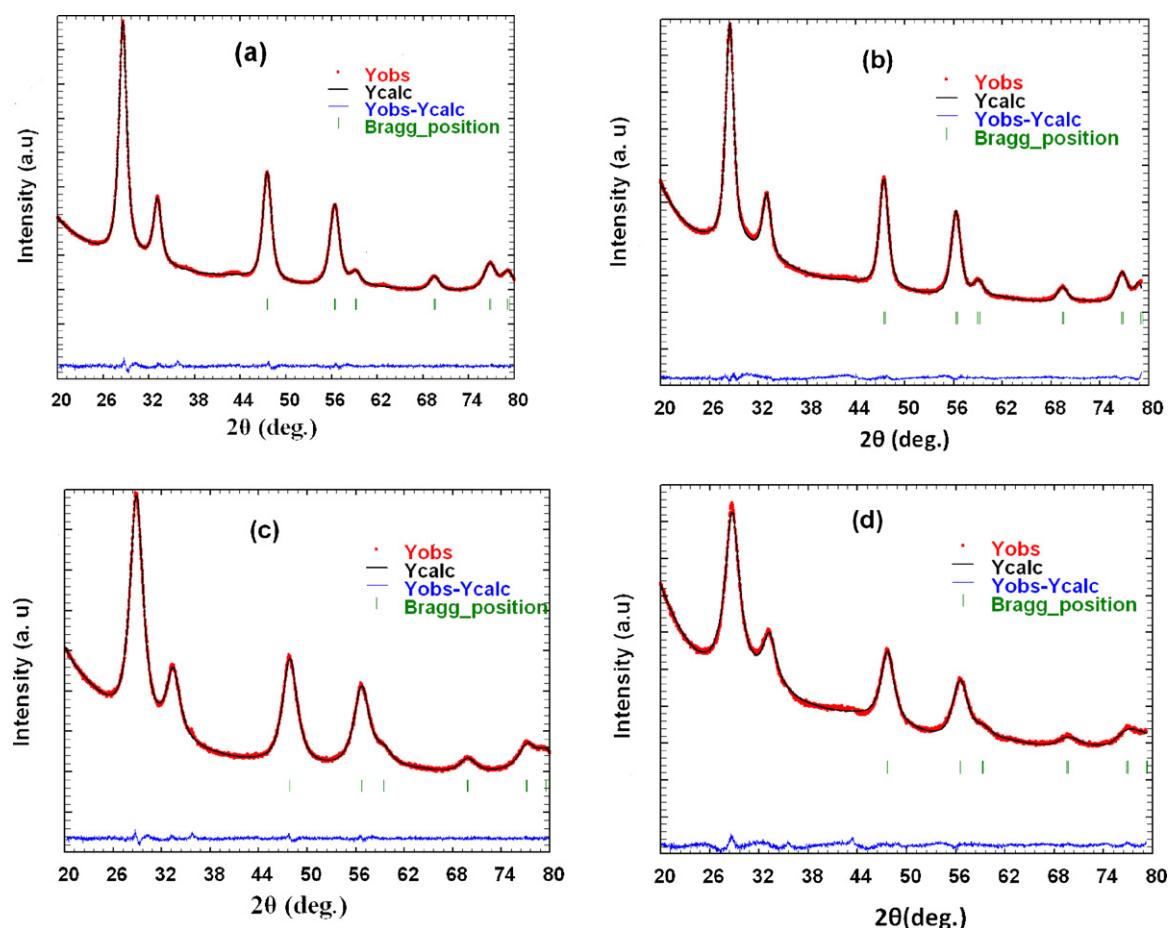


Fig. 1. Profile refined XRD patterns for $\text{Ce}_{0.75}\text{Cu}_{0.1}\text{Ni}_{0.15}\text{O}_{2-\delta}$ (a) before reaction, (b) after the reaction, respectively and for $\text{Ce}_{0.7}\text{Cu}_{0.1}\text{Fe}_{0.2}\text{O}_{2-\delta}$ (c) before the reaction, (d) after the reaction, respectively.

Bangalore, India), equipped with a FID and TCD detectors. 2 m long Haysep-A column was used to separate CO and CO_2 . CO and CO_2 were detected by FID incorporating a methanizer operating at 350°C using Ru catalyst. Conversion was calculated based on the FID signals representing CO and CO_2 . The rates were calculated from the CO and CO_2 concentrations and the material balance on carbon was within 3%. In all cases, the conversions were stable and highly reproducible ($\pm 1\%$). To determine the reaction rate and activation energy, all experiments were performed in order to establish differential reactor approach and mass transfer free operating conditions for each temperature. The rates were calculated from the slope of conversion with W/F. Thus, doubling the flow rate does not change the reaction rate. This indicates that the reaction kinetics were determined where there is no external mass transfer resistance. Because the particles were nano-sized, variation of sizes did not affect CO conversion indicating no internal mass transfer resistance. Experiments were carried out with a mixture of gases and different amounts of catalysts loading.

3. Results and discussion

3.1. Structural studies

Fig. 1 shows the XRD patterns for the synthesized compounds. All the diffraction patterns show peaks corresponding to the CeO_2 fluorite structure, even at higher concentrations of metal substitution. The XRD lines corresponding to various metal oxides of Cu, Ni and Fe were not observed in the powder pattern. The peaks corresponding to Cu, Fe metal was also absent. The crystal structure and the structural parameters of the synthesized compounds were determined by the profile refinement. The profile refinement was performed using the JANA 2000 suite program by taking Pseudo-Voigt as peak shape function and Legendre polynomial as background function (no. of terms = 15). This confirmed a single-phase fluorite type FCC structure (space group Fm3m, no. 225) without any impurity of Ce phases.

Fitting of the data to the cubic structure gave satisfactory values of the R_p and R_{wp} . The symbols in Fig. 1 show the experimental XRD

Table 1
Structural parameters for the ceria modified compounds obtained by profile refinement.

Compound	Lattice parameter (a)	R_p	R_{wp}	χ^2	Crystallite size (nm)
$\text{Ce}_{0.75}\text{Cu}_{0.1}\text{Ni}_{0.15}\text{O}_{2-\delta}$ (before reaction)	5.4031	1.98	1.49	3.18	12.2
$\text{Ce}_{0.75}\text{Cu}_{0.1}\text{Ni}_{0.15}\text{O}_{2-\delta}$ (after reaction)	5.4142	1.15	1.51	2.56	12.4
$\text{Ce}_{0.7}\text{Cu}_{0.1}\text{Fe}_{0.2}\text{O}_{2-\delta}$ (before reaction)	5.4083	1.72	1.91	1.04	7.5
$\text{Ce}_{0.7}\text{Cu}_{0.1}\text{Fe}_{0.2}\text{O}_{2-\delta}$ (after reaction)	5.4154	1.11	1.4	2.52	7.6

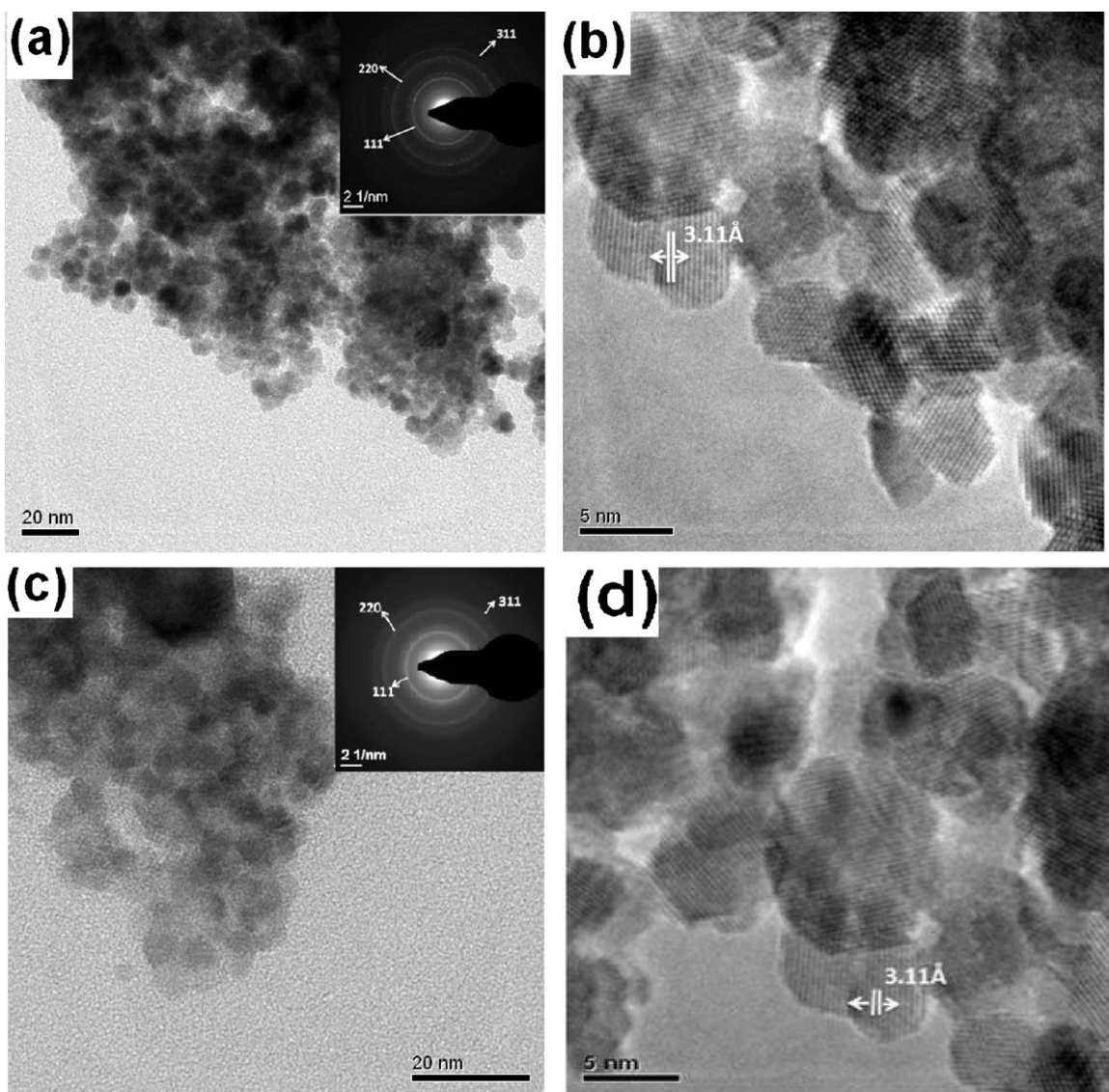


Fig. 2. (a) Bright field image and (b) HRTEM image of $\text{Ce}_{0.75}\text{Cu}_{0.1}\text{Ni}_{0.15}\text{O}_{2-\delta}$ and indexed electron diffraction pattern and enlarged view of lattice fringes in the inset of (a and b) respectively. (c) Bright field image and (d) HRTEM image of $\text{Ce}_{0.7}\text{Cu}_{0.1}\text{Fe}_{0.2}\text{O}_{2-\delta}$ and indexed electron diffraction pattern and enlarged view of lattice fringes in the inset of (c and d), respectively.

pattern, the solid lines show the predicted XRD pattern. The difference between the actual and theoretical pattern is shown by the light line at the bottom. The lattice parameters, crystallite size and the refinement reliability data for the both compounds are summarized in Table 1. The calculated lattice parameter, decreased on the substitution because bigger Ce^{4+} ions are replaced by smaller base metal ions. The observed XRD peaks are wide suggesting that the crystallites are nanometer in size and the average crystallite size was estimated using the Scherrer formula. The mean crystal size calculated from the full width half maxima (FWHM) of the strongest 111 diffraction peak was found to be 7.5 nm and 12.2 nm respectively, for $\text{Ce}_{0.75}\text{Cu}_{0.1}\text{Ni}_{0.15}\text{O}_{2-\delta}$ and $\text{Ce}_{0.7}\text{Cu}_{0.1}\text{Fe}_{0.2}\text{O}_{2-\delta}$.

The XRD patterns were recorded after the reaction as well to observe the changes in the crystal structure during the reaction. Figs. 1(b) and (d) show the profile refined XRD pattern of $\text{Ce}_{0.75}\text{Cu}_{0.1}\text{Ni}_{0.15}\text{O}_{2-\delta}$ and $\text{Ce}_{0.7}\text{Cu}_{0.1}\text{Fe}_{0.2}\text{O}_{2-\delta}$ respectively, after the reaction. The fluorite-type oxide diffraction pattern of CeO_2 was retained even after the reaction indicating that ceria is stable in the WGS reaction atmosphere. The reflections corresponding to any of metal oxide or metal were not detected in the XRD patterns. Table 1

summarizes the changes in the structural parameter after reaction derived from profile refinement. A slight increase in the lattice parameter of the spent catalysts compared to the as-synthesized catalysts indicates that the catalyst is in partially reduced state after reactions (discussed in XPS studies).

Fig. 2 shows the bright field and HRTEM images for $\text{Ce}_{0.75}\text{Cu}_{0.1}\text{Ni}_{0.15}\text{O}_{2-\delta}$ and $\text{Ce}_{0.7}\text{Cu}_{0.1}\text{Fe}_{0.2}\text{O}_{2-\delta}$. The electron diffraction patterns of respective compounds are also shown in the inset of Fig. 2. The ring type diffraction pattern was indexed to polycrystalline CeO_2 in fluorite structure and no diffraction line corresponding to any of the base metal oxides were detected suggesting the ionic substitution of these metals into ceria matrix. The width of the lattice fringes are 3.11 Å, which agrees well with the d_{111} planes of the fluorite $\text{Ce}_{0.75}\text{Cu}_{0.1}\text{Ni}_{0.15}\text{O}_{2-\delta}$ and $\text{Ce}_{0.7}\text{Cu}_{0.1}\text{Fe}_{0.2}\text{O}_{2-\delta}$. The bright field images show that individual crystallites sizes are 7 to 12 nm and 5 to 10 nm, respectively, for $\text{Ce}_{0.75}\text{Cu}_{0.1}\text{Ni}_{0.15}\text{O}_{2-\delta}$ and $\text{Ce}_{0.7}\text{Cu}_{0.1}\text{Fe}_{0.2}\text{O}_{2-\delta}$, which agrees well with the XRD measurements. The BET surface area for $\text{Ce}_{0.75}\text{Cu}_{0.1}\text{Ni}_{0.15}\text{O}_{2-\delta}$ and $\text{Ce}_{0.7}\text{Cu}_{0.1}\text{Fe}_{0.2}\text{O}_{2-\delta}$ was found to be 72 and 44 m^2/g , respectively.

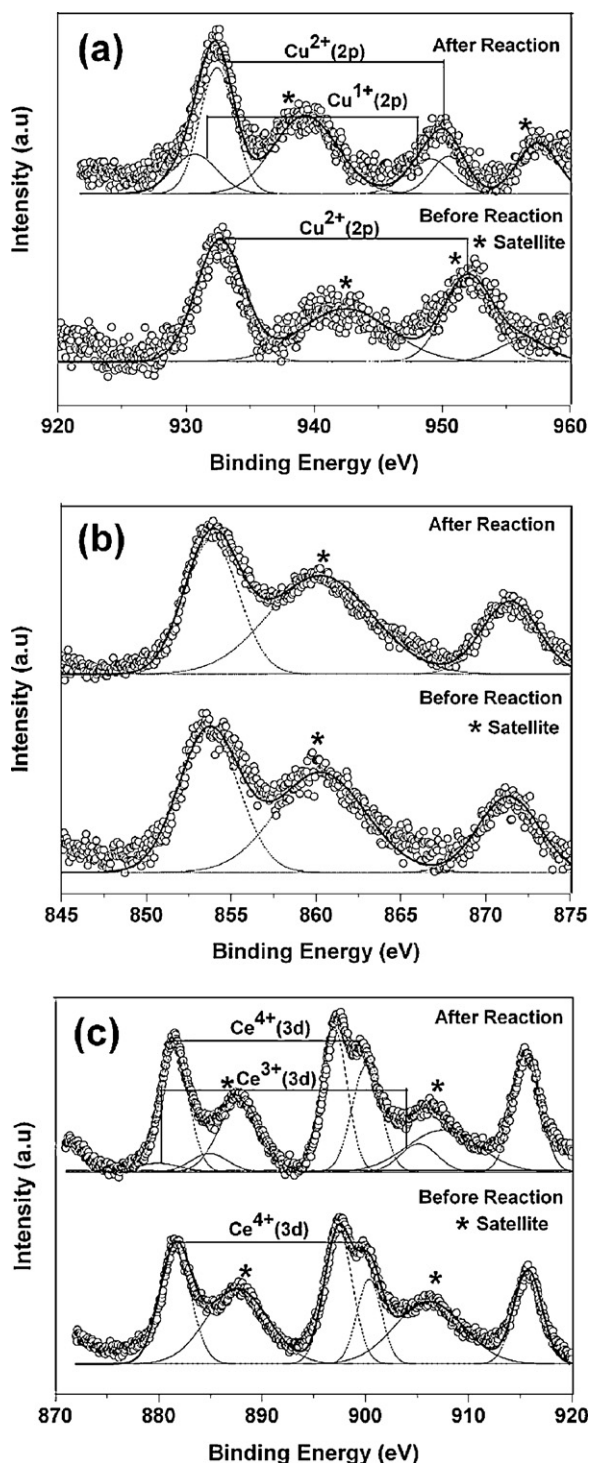


Fig. 3. Core level XPS of (a) Cu 2p, (b) Ni 2p, (c) Ce 3d in $\text{Ce}_{0.75}\text{Cu}_{0.1}\text{Ni}_{0.15}\text{O}_{2-\delta}$.

The metal support interactions and possible surface processes were established by tracing the changes in the electronic structure of the compounds using XPS. The oxidation states of the base metals in the compounds were found by XPS. The spectra were recorded both before and after the reaction. Fig. 3(a) and Fig. 4(a) show the Cu 2p spectra in $\text{Ce}_{0.75}\text{Cu}_{0.1}\text{Ni}_{0.15}\text{O}_{2-\delta}$ and $\text{Ce}_{0.7}\text{Cu}_{0.1}\text{Fe}_{0.2}\text{O}_{2-\delta}$, respectively, before and after the reaction. The binding energies were calibrated with respect to the binding energy of graphite observed at 285 eV. Cu ($2p_{3/2}, 1/2$) peaks were resolved into sets of spin-orbit doublets. The Cu oxidation state was determined on

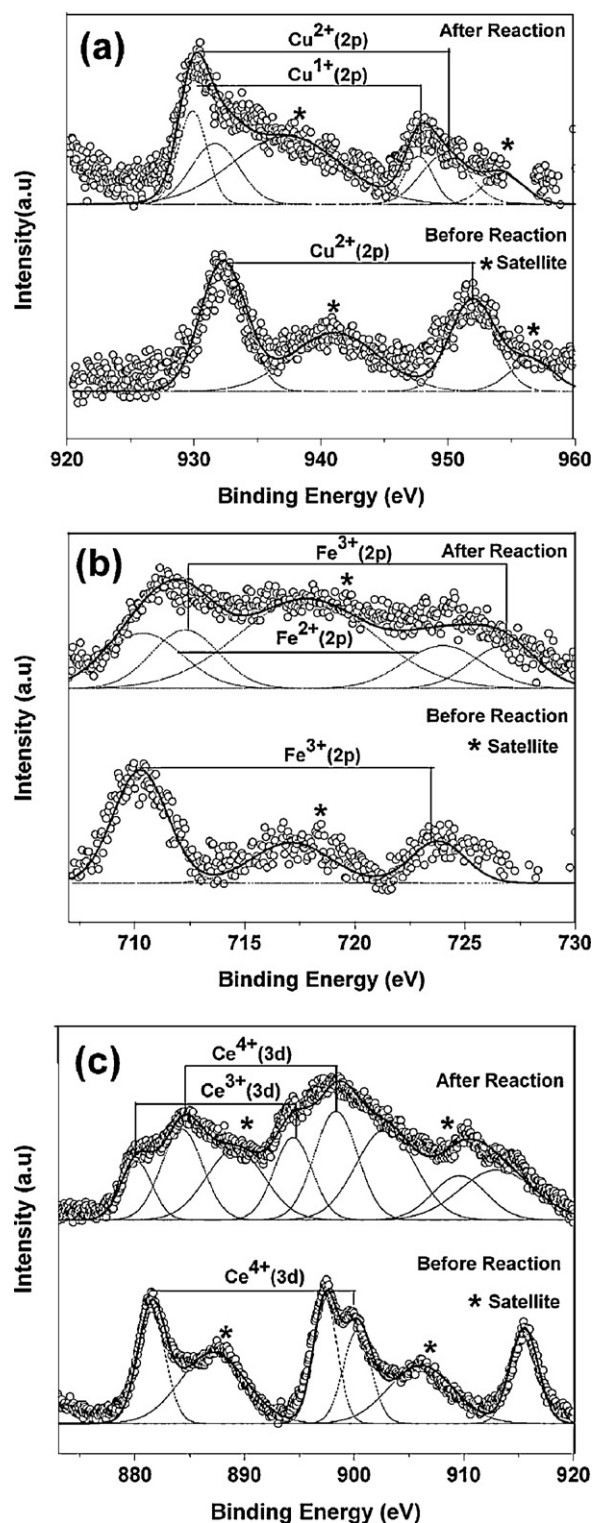


Fig. 4. Core level XPS of (a) Cu 2p, (b) Fe 2p, (c) Ce 3d in $\text{Ce}_{0.7}\text{Cu}_{0.1}\text{Fe}_{0.2}\text{O}_{2-\delta}$.

the assumption that Cu^{2+} and Cu^{1+} could be distinguished by the presence of the satellite peak in Cu 2p spectra. The Cu ($2p_{3/2}, 1/2$) peaks at 934.0 and 953.8 eV with satellites at 9 eV below the main peak in both as-synthesized compounds can only be assigned to Cu in the 2+ oxidation state [31] indicating ionic substitution of Cu in the ceria lattice. X-ray photoelectron spectra of the both samples after the reaction were wide indicating multiple oxidation states of Cu species. Therefore, the spectra were de-convoluted to obtain

the individual peaks corresponding to Cu^{2+} and Cu^{1+} species. In the de-convoluted Cu (2p) spectra of the spent catalysts, the Cu ($2p_{3/2}$) peak at 932.8 eV along satellite peak indicates the presence of mixed $\text{Cu}^{2+}/\text{Cu}^{1+}$ species.

The core level Ni (2p) spectra of $\text{Ce}_{0.75}\text{Cu}_{0.1}\text{Ni}_{0.15}\text{O}_{2-\delta}$ compound before and after the reaction are shown in Fig. 3(b). The features of the Ni $2p_{3/2}$ core level of the $\text{Ce}_{0.75}\text{Cu}_{0.1}\text{Ni}_{0.15}\text{O}_{2-\delta}$ compound and the observed peak position of 854 eV is clearly different from that of NiO. This confirms that the Ni ion in the $\text{Ce}_{0.75}\text{Cu}_{0.1}\text{Ni}_{0.15}\text{O}_{2-\delta}$ compound is not present as NiO and the chemical environment of the substituted Ni ions in the $\text{Ce}_{0.75}\text{Cu}_{0.1}\text{Ni}_{0.15}\text{O}_{2-\delta}$ compound is different from that of the Ni ions in NiO. The present interpretation of Ni 2p spectra of oxides is based on the main peak at 854 eV and the broad satellite centered at around 860 eV. Therefore Ni was present in the 2+ state in as-synthesized compound [32]. After reaction, no appreciable changes were observed in Ni (2p) spectrum and Ni remains in the 2+ oxidation state in the spent catalyst.

Fig. 4(b) presents the Fe (2p) XPS spectra of the $\text{Ce}_{0.7}\text{Cu}_{0.1}\text{Fe}_{0.2}\text{O}_{2-\delta}$ before and after the reaction. Fe 2p spectrum of the as-synthesized compound shows a large peak at a binding energy of 711.4 eV along with the satellite peak at higher binding energy (between 715 and 720 eV), which is characteristic of Fe^{3+} species. Thus, Fe is mainly present in the 3+ oxidation state in the as-synthesized catalyst. However, the wider Fe ($2p_{3/2}$) peak in the case of the spent catalyst compared to the as-synthesized catalyst suggests that a small percentage of Fe^{2+} is also present in the spent catalyst. This indicates that the presence of reducing atmosphere causes the partial reduction of Fe^{3+} to Fe^{2+} [33].

The spectra of the Ce (3d) before and after reaction are shown in Fig. 3(c) and Fig. 4(c), respectively, for $\text{Ce}_{0.75}\text{Cu}_{0.1}\text{Ni}_{0.15}\text{O}_{2-\delta}$ and $\text{Ce}_{0.7}\text{Cu}_{0.1}\text{Fe}_{0.2}\text{O}_{2-\delta}$. The interpretation of the Ce 3d spectra is more complicated than that of the Cu 2p spectra due to multiplet splitting. Six peaks corresponding to three pairs of spin-orbit doublets can be identified in the Ce 3d spectrum from as-synthesized compounds. The Ce ($3d_{5/2}$) peak was observed at 882.7 eV along with satellite peaks at 6.4 and 16 eV from the main peak, which are characteristic peaks of Ce^{4+} in CeO_2 [31]. Thus, in both the as-synthesized compounds, Ce was present mainly in 4+ state. After the reaction, the spectra were wide indicating partial reduction of catalyst surface. Therefore, the Ce (3d) spectrum was resolved into Ce^{3+} and Ce^{4+} components. 10 peaks were identified; 3 doublets resulting from CeO_2 and 2 doublets resulting from Ce_2O_3 . Ce^{3+} (3d) in Ce_2O_3 is characterized by Ce ($3d_{5/2}$) at 883.3 eV along with an intense satellite at 887.1 eV [31]. Thus Ce is found to be in mixed states of 4+ and 3+.

3.2. H_2 -TPR experiments

Ceria is known to be an oxygen storage material and capable of being readily reduced and re-oxidized. TPR was used to study the influence of ionic substitution of base metal on ceria reducibility. This analysis revealed that the binding energy (bond strength) between the metal cation and oxygen anion is substantially weakened due to the presence of base metals and its reduction temperature is lowered by several hundred degrees. H_2 -TPR (H_2 uptake) profiles over $\text{Ce}_{0.75}\text{Cu}_{0.1}\text{Ni}_{0.15}\text{O}_{2-\delta}$ and $\text{Ce}_{0.7}\text{Cu}_{0.1}\text{Fe}_{0.2}\text{O}_{2-\delta}$ as a function of temperature are shown in Fig. 5. The presence of base metal facilitates the surface reduction of ceria at much lower temperature. The two peaks below 300 °C have been reported for copper substituted ceria and assigned to the isolated $-\text{Cu}^{2+}-\text{O}-\text{Cu}^{2+}-$ dimer and Cu^{2+} ions from the $-\text{Cu}^{2+}-\text{O}-\text{Ce}^{4+}-$ type of species present in the Cu/CeO₂ catalyst material [31]. In case of $\text{Ce}_{0.75}\text{Cu}_{0.1}\text{Ni}_{0.15}\text{O}_{2-\delta}$, the H_2 consumption was observed in the temperature range between 325 and 350 °C and can be assigned

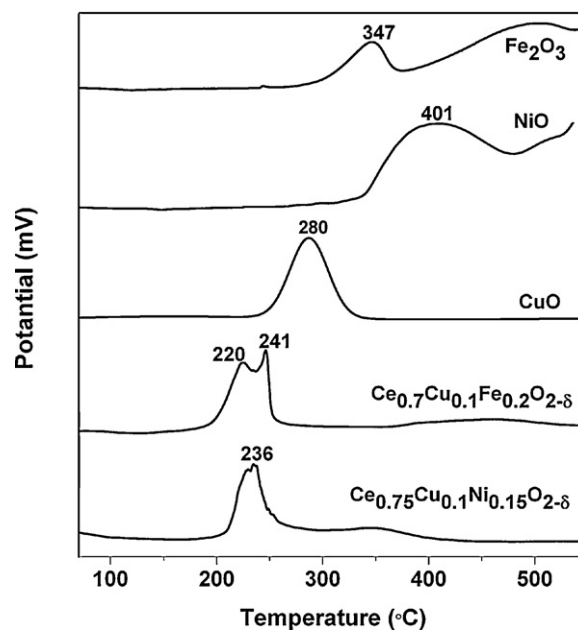


Fig. 5. H_2 /TPR profile for ceria modified compounds and various base metal oxides.

to the reduction of Ni^{2+} species. The comparison between NiO and $\text{Ce}_{0.75}\text{Cu}_{0.1}\text{Ni}_{0.15}\text{O}_{2-\delta}$ indicates that Ni species substituted in CeO_2 shows higher reducibility than that of pure NiO. This means that the lower temperature shift of H_2 consumption peak on the substitution in CeO_2 can be explained by the strong interaction between Ni species and CeO_2 .

In case of $\text{Ce}_{0.7}\text{Cu}_{0.1}\text{Fe}_{0.2}\text{O}_{2-\delta}$, the H_2 consumption at lower temperature is due to the reduction of Cu^{2+} ions, while the reduction peak at higher temperature is due to the reduction of Fe^{3+} ions. No distinct reduction peaks due to iron oxide species were observed. The area under the peaks corresponding to the reduction of surface oxygen of $\text{Ce}_{0.75}\text{Cu}_{0.1}\text{Ni}_{0.15}\text{O}_{2-\delta}$ compound is higher than $\text{Ce}_{0.7}\text{Cu}_{0.1}\text{Fe}_{0.2}\text{O}_{2-\delta}$, indicating $\text{Ce}_{0.75}\text{Cu}_{0.1}\text{Ni}_{0.15}\text{O}_{2-\delta}$ is more reducible than $\text{Ce}_{0.7}\text{Cu}_{0.1}\text{Fe}_{0.2}\text{O}_{2-\delta}$. The H_2 -TPR profile of the metal oxide such as CuO, Fe_2O_3 and NiO are also shown in Fig. 5 for comparison. The peak reduction temperatures of metal oxides are different from ceria substituted compounds, which shows the formation of complete solid solution of ceria and base metals. This also indicates the absence of the respective metal oxides phase in both of ceria modified compounds.

3.3. OSC

Cyclic H_2 -TPR was conducted to determine the reversibility of modified ceria structures in redox treatment and this was correlated with activity of catalyst towards WGS reaction. OSC of both catalysts was calculated by the hydrogen uptake. The catalyst sample (calcined in air at 300 °C for 1 h) was reduced in 5% H_2/Ar up to 600 °C (C1), and then re-oxidized in air at 300 °C for 30 min. The H_2 -TPR cycle was repeated (C2) after purging in N_2 for 30 min. Similarly, re-oxidation was also done in air at 200 °C and the OSC was calculated (C3). The histograms corresponding to these successive cycles for both compounds are shown in Fig. 6. H_2 consumption up to 400 °C for the first, second and third run is 1051, 788 and 609 $\mu\text{mol/g}$, respectively for $\text{Ce}_{0.75}\text{Cu}_{0.1}\text{Ni}_{0.15}\text{O}_{2-\delta}$ and 761, 690 and 530 $\mu\text{mol/g}$ respectively, for $\text{Ce}_{0.7}\text{Cu}_{0.1}\text{Fe}_{0.2}\text{O}_{2-\delta}$. The fresh sample showed the highest OSC and a slight decrease in the OSC was observed in the subsequent cycles. The OSC in three consecutive cycles follows the order: $\text{C3} < \text{C2} < \text{C1}$. It has been reported that irreversible changes occur to $\text{Au}/\text{Fe}_2\text{O}_3$ [34] and Au/TiO_2 [35]

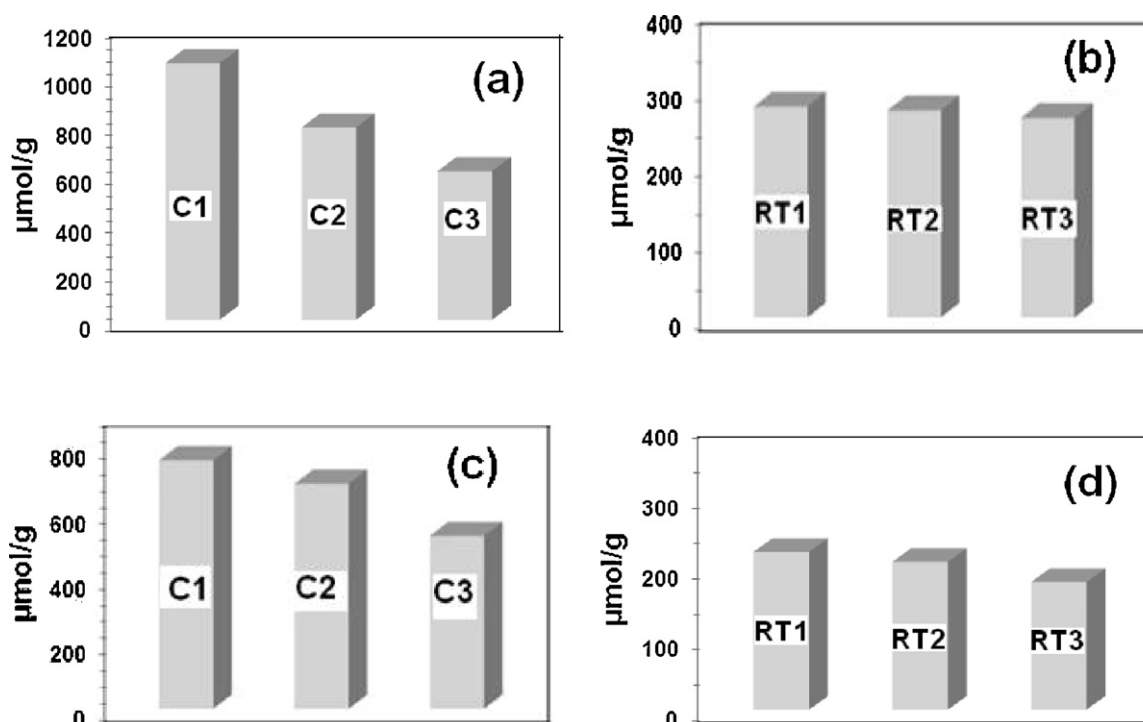


Fig. 6. OSC of ceria based compounds of oxidized sample at various temperatures after three consecutive cycles.

after reduction, which might attributed to the deactivation of these catalysts. In this study, we report on the reversibility of ceria modified structures at various temperatures. The H_2 -TPR indicates that after the first reduction by H_2 up to 600 °C, some irreversible surface changes occurred. However, the surface structures of modified ceria catalysts are highly reducible and can be re-oxidized by O_2 in great extent. It is well known that CuO reduced to Cu metal does not get oxidized to CuO in the presence of pure O_2 and hydrogen uptake in the second cycle in the H_2 -TPR of CuO is not expected. Therefore, it seems that Cu^{2+} ions in ceria modified catalysts shows a redox cycle, unlike the case for CuO [31]. If only Cu^{2+} had been reduced to the Cu^0 state, the H/Cu ratio should have been 2 but the H/Cu ratio was found to be 6 and 4.34 respectively, for $Ce_{0.75}Cu_{0.1}Ni_{0.15}O_{2-\delta}$ and $Ce_{0.7}Cu_{0.1}Fe_{0.2}O_{2-\delta}$ catalysts (up to 400 °C). This higher H/Cu ratio can be assigned to a hydrogen spillover from Cu^{2+} ions to neighboring Ni^{2+}/Fe^{3+} and Ce^{4+} ions. The spillover of H_2 over Cu based catalyst can be found in the literature as well [36]. The H/Cu ratios corresponding to each TPR cycle are given in Table 2 for both the catalysts.

After the first H_2 -TPR experiment of fresh sample, the reoxidation was also carried out 25 °C at room temperature. The sample was cooled to 25 °C in pure Ar, and re-oxidized in the air at 25 °C for 30 min; the H_2 -TPR experiment was performed again. Thus, OSC obtained after three consecutive cycles is presented in Fig. 6. It should be noted that in both the compounds, the re-oxidation and reasonably good OSC are manifested. The results obtained in this study indicates that the reduction/oxidation processes take place at significantly lower temperatures, even at 25 °C over these base metal modified ceria catalysts. The presence of base metals

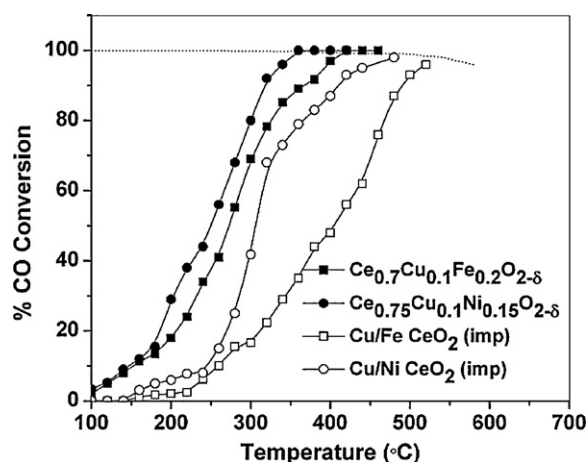


Fig. 7. WGS activity of various ceria-based compounds with temperature.

facilitates both the restoration of the surface oxygen anions and their removal by H_2 at lower temperatures. This results in the high activity of the ionic base metal substituted ceria systems for the low-temperature WGS reaction.

3.4. Activity studies

The activity of catalyst is expressed in terms of percentage of CO conversion. Fig. 7 shows the steady-state CO conversions over $Ce_{0.75}Cu_{0.1}Ni_{0.15}O_{2-\delta}$ and $Ce_{0.7}Cu_{0.1}Fe_{0.2}O_{2-\delta}$ in a feed gas of 2 vol%

Table 2

Hydrogen atoms consumed per copper (H/Cu) atom in the H_2 -TPR experiment for ceria modified catalyst.

	300 °C			RT		
	C1	C2	C3	RT1	RT2	RT3
$Ce_{0.75}Cu_{0.1}Ni_{0.15}O_{2-\delta}$	6	4.5	3.47	1.57	1.54	1.49
$Ce_{0.7}Cu_{0.1}Fe_{0.2}O_{2-\delta}$	4.34	3.93	3.02	1.27	1.19	1.02

Table 3
Reaction rates and activation energies for the WGS reaction on various supported catalysts and corresponding reaction conditions (gas composition, temperature range).

Catalyst	Gas composition	Rate ($\mu\text{mol/g/s}$) ($^{\circ}\text{C}$)	Activation energy (kJ/mol)	Reference
Cu/ZnO/Al ₂ O ₃	1% CO, 2% H ₂ O	0.12 (100)	53	37
Au/Fe ₂ O ₃	1% CO, 2% H ₂ O	0.022 (100)	52	37
Au/TiO ₂	1% CO, 2% H ₂ O	0.3 (100)	31, 46 ^a	37
Pd/CeO ₂	25 Torr CO, 25 Torr H ₂ O	5.6 (180)	48	5
Pd/Al ₂ O ₃	25 Torr CO, 25 Torr H ₂ O	0.18 (180)	65	5
Ni/CeO ₂	24 Torr CO, 22 Torr H ₂ O	1.6 (225–275)	44	38
Pd/CeO ₂	24 Torr CO, 22 Torr H ₂ O	1.5 (225–275)	38	38
5% at Ni–Ce(10%La)O _x	1% CO, 2% H ₂ O	0.6 (175–300)	38.2	9
Au/CeO ₂	1% CO, 2% H ₂ O	0.2 (100)	34	39
Ce _{0.7} Cu _{0.1} Fe _{0.2} O _{2–δ}	1.3% CO, 35% H ₂ O	1.7 (240)	37	(Present study)
Ce _{0.75} Cu _{0.1} Ni _{0.15} O _{2–δ}	1.3% CO, 35% H ₂ O	2.2 (240)	32	(Present study)

^a Depending on the preparation conditions.

CO balanced with N₂ keeping total flow rate at 100 ml/min. The flow rate of H₂O vapor was maintained at 55 ml/min. The WGS light-off temperature of both modified ceria samples is below 200 $^{\circ}\text{C}$, while ceria itself is inactive below 300 $^{\circ}\text{C}$. The Ce_{0.75}Cu_{0.1}Ni_{0.15}O_{2–δ} sample shows the higher reactivity than Ce_{0.7}Cu_{0.1}Fe_{0.2}O_{2–δ}, in agreement with the OSC data in Fig. 6. The lower activity exhibited by the Ce_{0.7}Cu_{0.1}Fe_{0.2}O_{2–δ} catalyst can be explained by the fact that Fe metal are likely to be oxidized under reaction conditions and therefore unlikely to stabilize CO adsorption. Products from possible side reactions such as CH₄ and other hydrocarbons were not detected in the product stream within the detection limit of 5 ppm. Due to the ionic substitution of base metal in ceria modified catalysts, these showed much higher activity for WGS than bare ceria. The complete conversion of CO to CO₂ with 100% H₂ selectivity was achieved at 320 $^{\circ}\text{C}$ for Ce_{0.75}Cu_{0.1}Ni_{0.15}O_{2–δ} and 380 $^{\circ}\text{C}$ for Ce_{0.7}Cu_{0.1}Fe_{0.2}O_{2–δ} and, no decrease in CO conversion was observed during reaction.

The rate of reaction and activation energy was measured by carrying out the WGS reaction with varying amounts of catalyst keeping the total gas flow at 100 ml/min. The temperature of reactor was varied in such way that differential reactor approach is applicable. The rates of reaction were determined using the following equation:

$$\text{Rate}(r) = \frac{F \times x}{W} = \frac{x}{W/F} \quad (1)$$

where F is the flow of the gas in mol/s, W is the weight of the catalyst in g and x is the fractional CO conversion. The variation of the fractional CO conversion (x) with W/F plot for the Ce_{0.75}Cu_{0.1}Ni_{0.15}O_{2–δ} and Ce_{0.7}Cu_{0.1}Fe_{0.2}O_{2–δ} catalysts is shown in Fig. 8(a) and (b), respectively. The fractional conversion (x) with W/F plot is linear up to 50% conversion. The rates of reaction over all catalysts were calculated at various temperatures from the slope of linear portion. The rate of reaction as function of temperature is shown in Fig. 8(c) and (d) respectively for Ce_{0.75}Cu_{0.1}Ni_{0.15}O_{2–δ} and Ce_{0.7}Cu_{0.1}Fe_{0.2}O_{2–δ} catalysts. The higher rate was observed over Ce_{0.75}Cu_{0.1}Ni_{0.15}O_{2–δ} compared to Ce_{0.7}Cu_{0.1}Fe_{0.2}O_{2–δ}. The apparent activation energy was calculated from the Arrhenius equation plot (see inset of Fig. 8(c) and (d) respectively, for Ce_{0.75}Cu_{0.1}Ni_{0.15}O_{2–δ} and Ce_{0.7}Cu_{0.1}Fe_{0.2}O_{2–δ} catalysts). The apparent activation energies for Ce_{0.75}Cu_{0.1}Ni_{0.15}O_{2–δ} and Ce_{0.7}Cu_{0.1}Fe_{0.2}O_{2–δ} are 32 and 37 kJ/mol, respectively. The comparison of reaction rate and activation energy along with gas composition of various catalysts examined in previous studies is given in Table 3 [5,9,37–39]. The rate of reaction expressed here is in mol/g.s. If rate was calculated based on the surface area, i.e. mol/m²s then the activity of Ce_{0.7}Cu_{0.1}Fe_{0.2}O_{2–δ} would be higher than that of Ce_{0.75}Cu_{0.1}Ni_{0.15}O_{2–δ}.

The WGS reaction is equilibrium limited and CO conversion is mainly governed by the thermodynamics at higher temperatures

rather than kinetics. The shift in the equilibrium to the left side reduces the CO conversion and this can happen only if the adsorption of CO₂ and H₂ is significant. We did not observe the decrease in CO conversion as function of temperature over these catalysts and it seems that these catalysts do not support a reverse WGS reaction. To investigate this, a reverse WGS reaction over the Ce_{0.75}Cu_{0.1}Ni_{0.15}O_{2–δ} and Ce_{0.7}Cu_{0.1}Fe_{0.2}O_{2–δ} catalysts was also carried out both in the presence and absence of feed H₂O. A reverse WGS reaction was carried out in absence of H₂O with 2 vol% CO₂, 2 vol% H₂ and balance of N₂ to make total flow rate of 100 ml/min over 300 mg of the catalyst. The concentrations of CO₂ and H₂ are shown as a function temperature in the Fig. 9(a) and (c), respectively, for Ce_{0.75}Cu_{0.1}Ni_{0.15}O_{2–δ} and Ce_{0.7}Cu_{0.1}Fe_{0.2}O_{2–δ}. The concentrations were normalized by the initial concentration of CO₂. In the absence of feed H₂O, CH₄ formation was observed above 260 $^{\circ}\text{C}$ in addition to CO formation over Ce_{0.75}Cu_{0.1}Ni_{0.15}O_{2–δ} and in case of Ce_{0.7}Cu_{0.1}Fe_{0.2}O_{2–δ}, CO formation was observed from 400 $^{\circ}\text{C}$ onwards. CH₄ formation was not observed over Ce_{0.7}Cu_{0.1}Fe_{0.2}O_{2–δ} in the studied temperature range up to 500 $^{\circ}\text{C}$. The experiment was carried in presence of H₂O with the same gas composition as that used in the absence of H₂O over 300 mg of the catalyst. 55 ml/min of H₂O vapor was introduced along with the reaction mixture. The normalized CO₂ and H₂ concentration as a function of temperature is shown in Fig. 9(b) and (d), respectively, for Ce_{0.75}Cu_{0.1}Ni_{0.15}O_{2–δ} and Ce_{0.7}Cu_{0.1}Fe_{0.2}O_{2–δ}. CO formation does not occur over either of these catalysts and no measurable decrease in the concentration of H₂ and CO₂ was observed even up to 500 $^{\circ}\text{C}$. In presence of H₂O, methanation activity was not observed over Ce_{0.75}Cu_{0.1}Ni_{0.15}O_{2–δ} catalyst. Thus, in the presence of excess H₂O in the reaction stream, a reverse WGS reaction does not occur over these catalysts. This indicates that high concentration of H₂O vapors in the reaction stream suppresses CO₂ absorption over these catalysts. However, the absence of H₂O vapors facilitates a reverse WGS reaction and methane formation. This may also be due to preserving the base metal in the ionic state under the WGS reaction conditions (see Figs. 3 and 4). Metallic species are known catalysts for methanation and Fischer-Tropsch activity [40].

Further, to show that ionic ceria modified catalyst facilitates ease removal of lattice oxygen, WGS reaction was also carried out over base metal impregnated ceria and the activity compared with those of ionic substituted ceria catalysts. The activity of these compounds towards WGS reaction was measured with 2 vol% of CO and balance of N₂ with a total flow of 100 ml/min over 300 mg of catalyst and % CO conversion as functions of temperature is shown in Fig. 7 for both the impregnated catalysts. Ceria impregnated catalysts display a several-fold lower activity than the ionic ceria catalyst. A nearly complete conversion of CO to CO₂ (~98%) was observed around 440 $^{\circ}\text{C}$ for impregnated Cu/Ni/CeO₂ and around 500 $^{\circ}\text{C}$ for impregnated Cu/Fe/CeO₂ compared to 320 $^{\circ}\text{C}$ for Ce_{0.75}Cu_{0.1}Ni_{0.15}O_{2–δ} and 380 $^{\circ}\text{C}$ for Ce_{0.7}Cu_{0.1}Fe_{0.2}O_{2–δ}. It means

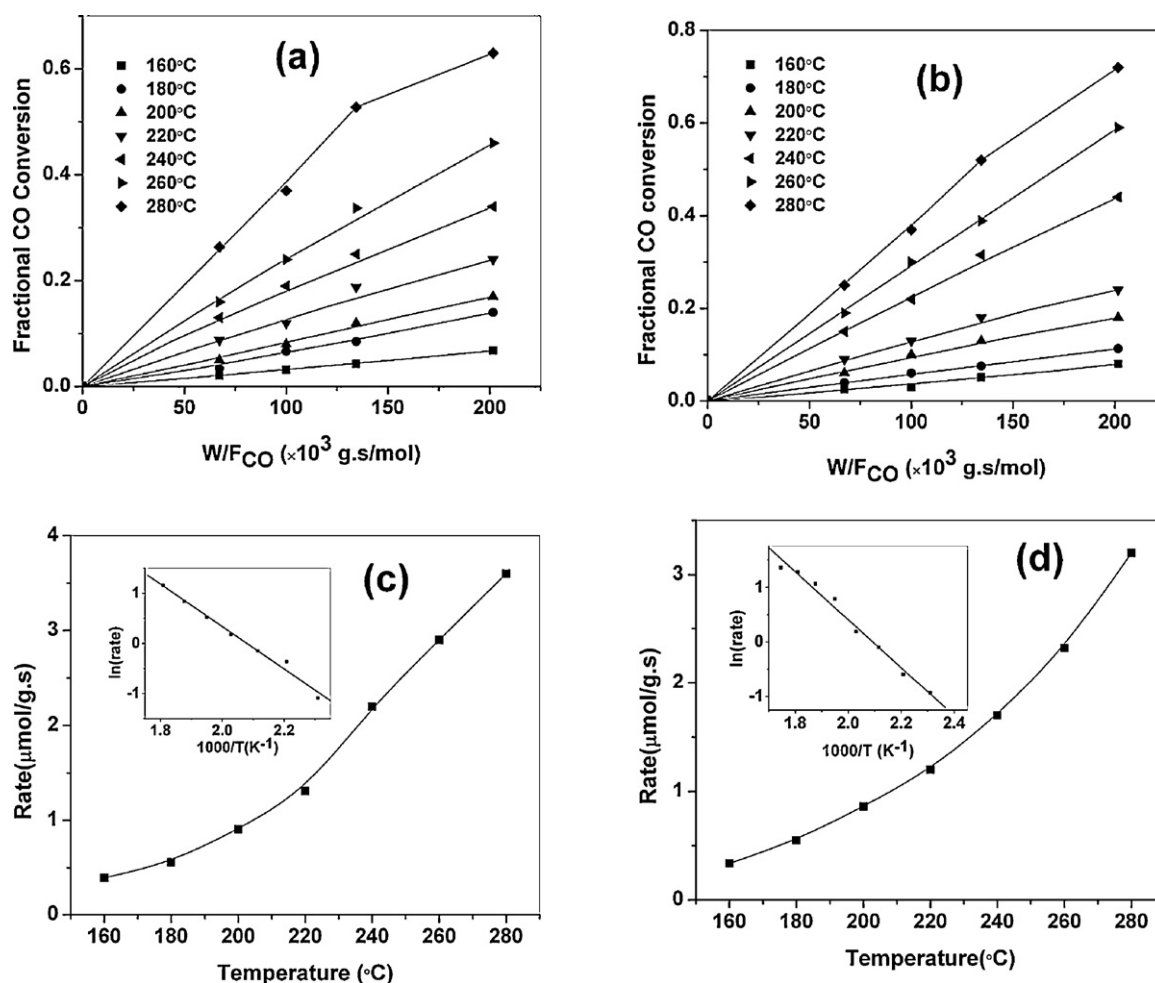


Fig. 8. Variation of fractional conversion of CO with W/F_{CO} for (a) $Ce_{0.75}Cu_{0.1}Ni_{0.15}O_{2-\delta}$, (b) $Ce_{0.7}Cu_{0.1}Fe_{0.2}O_{2-\delta}$ and rate of reaction as function of temperature for (c) $Ce_{0.75}Cu_{0.1}Ni_{0.15}O_{2-\delta}$ and (d) $Ce_{0.7}Cu_{0.1}Fe_{0.2}O_{2-\delta}$.

that the ionic ceria catalyst shows higher activity than those of impregnated ceria catalysts due to increase in the amount of surface oxygen in ceria.

3.5. Kinetic model

Numerous studies on the reaction kinetics and mechanisms for the WGS reaction have been reported in the literature. The two

distinctly different kinetic mechanisms namely adsorptive mechanism and redox mechanism have been proposed. The adsorptive mechanism involves competitive adsorption of CO and H_2O on the catalyst surface and formation of an intermediate such as formate, which decomposes as desorbed products. The existence of this intermediate was evidenced through chemical trapping experiments, isotopic labeling or IR spectroscopy [41–44]. This proposal was based on a comparison of the rates for the WGS reaction and

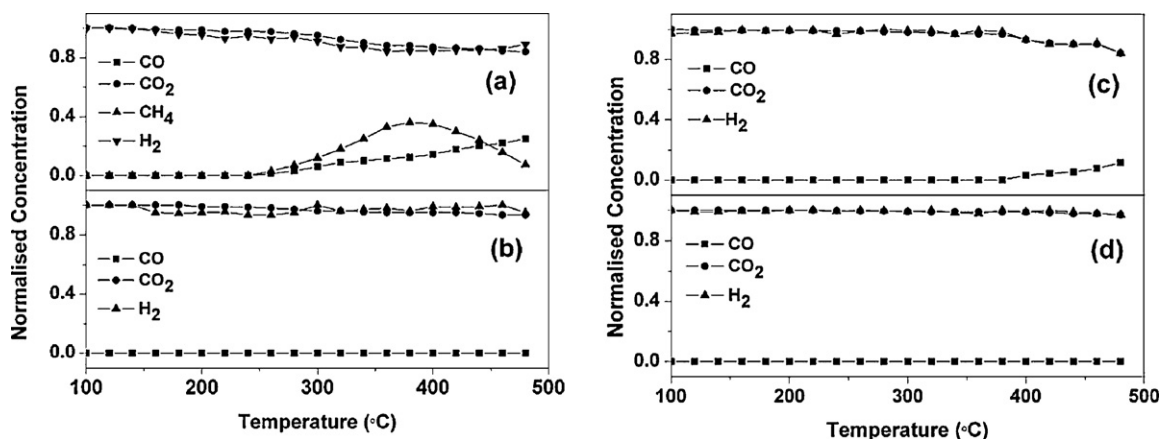
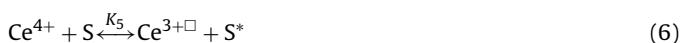


Fig. 9. Normalized CO_2 , H_2 and CO concentrations in reverse WGS reaction over $Ce_{0.75}Cu_{0.1}Ni_{0.15}O_{2-\delta}$ (a) in absence of H_2O , (b) in presence of H_2O , respectively and normalized CO_2 , H_2 and CO concentrations in reverse WGS reaction over $Ce_{0.7}Cu_{0.1}Fe_{0.2}O_{2-\delta}$ (c) in absence of H_2O , (d) in presence of H_2O , respectively.

formic acid decomposition [38,45,46]. The quantitative evidence based on transient isotopic work has also been provided for the redox vs. associative mechanism of WGS over Pt/CeO₂ [47]. Most recently, carbonate species were proposed to be the reaction intermediate for the reverse WGS reaction, based on steady state isotope exchange measurements [48–51]. On the other hand, the redox mechanism involves the reduction of catalyst by CO in the first step and subsequent catalyst oxidation by H₂O in the second step [52]. Despite the vast literature on the WGS reaction, there is no unanimity over the active site and the reaction mechanism.

This study underscores the important link between CO conversion and the extent of ceria reducibility. It is well known that the reduction of ceria is facilitated by the presence of the base metal promoter. An increase in the number of reduced centers (vacancies) is expected to improve the density of active sites. Therefore, the possibility of a redox mechanism cannot be ruled out [5] and a wide variety of ceria-mediated redox mechanism can be found in the literature [9,20,38]. Secondly, if adsorptive mechanism was operative, WGS reaction rates would probably exhibit a maximum at relatively low temperatures due to limited thermal stability of formates [21]. However, Fig. 7 clearly shows that WGS rates increase steadily with increasing temperature. Thirdly, it has been reported in the literature that each of the proposed mechanistic steps with the redox mechanism was observed in pulse-reactor measurements at 450 °C, a temperature above which the formate is reported to be stable [5]. The enhancement in the activity of Pd/ceria in comparison with Pd/alumina indicates that formate might be spectator species at this temperature [53–55]. We also confirmed this kind of redox mechanism by passing CO over 300 mg of the catalyst at 250 °C for 30 min. CO₂ was observed in the output stream via utilization of lattice oxygen. Then, H₂O vapor with N₂ was allowed to pass over the catalyst at the same temperature and H₂ formation was indeed observed. This indicates that the redox mechanism is operative over these catalysts.

Based on the above discussion and spectroscopic analysis, a synergistic redox model has been proposed. The CO molecules adsorbed on the metal cations react with adjacent surface lattice oxygen. H₂O dissociates on an oxygen vacancy site of ceria to H₂ and atomic oxygen, which re-oxidizes the ceria. Ample evidences of the redox reaction mechanism are found in oxidation reactions over ceria-supported metal-metal oxides and this is not limited only to noble metals on ceria [9]. The redox mechanism over Cu surfaces for the LTS reaction has previously been studied extensively by Campbell et al. [56] and modeled by Ovesen et al. [57]. Though a reversible WGS reaction does not occur over these catalysts, an attempt was made to develop an exhaustive mechanism, which accounts for the reversibility of reaction as well. This model demonstrates the importance of oxygen storage capacity and oxygen mobility in these catalysts. The overall reaction can be written as



“S*” and “S” represent the metal cation either Cu²⁺ or Fe³⁺ ions and Cu¹⁺ or Fe²⁺, ions respectively. Ce^{3+□} and Ce⁴⁺ represent reduced ceria (oxide vacancy) and oxidized ceria, respectively. The first step of mechanism involves the adsorption of CO onto the metal cation to form an intermediate (equation (2)). The reaction of this adsorbed intermediate with lattice oxygen leads to the formation of oxygen vacancy (equation (3)). Thus, the oxygen balance in equation (3) arises from S* reducing to S (i.e. Cu²⁺ is reduced to Cu¹⁺ and this oxygen oxidizing CO to CO₂). Thus, these results in the formation of reduced ceria surface. The catalyst surface rejuvenated in the oxidizing environment provided by H₂O, releasing H₂ (equation (5)). Since the molecular adsorption of H₂O on metals is weak [39], we can assume that H₂O adsorption and dissociation occur only on the ceria surface. The oxidation of reduced CeO₂ by H₂O to give H₂ is thermodynamically favorable and has been also observed in low pressure adsorption studies [21]. Reversibility of equations (2) and (4) can be justified by the fact that CO and H₂O molecules have high sticking probabilities, very low dissociation probabilities and small heats of adsorption over base metal so that the equilibria are very rapidly established [58].

Equation (6) represents the redox reaction between Ce ion and metal cation to maintain charge neutrality of lattice. This step can be envisaged because of metal cations are in the ionic form. The XPS studies before and after reaction have demonstrated that due to ionic substitution of Fe and Cu in the ceria, additional redox couple namely, Fe³⁺ ↔ Fe²⁺ and Cu²⁺ ↔ Cu¹⁺ can function, which results in the creation more oxide vacancies. These vacancies are highly effective for the complete dissociation of H₂O into H₂ and adsorbed oxygen under reaction conditions. In case of Ce_{0.75}Cu_{0.1}Ni_{0.15}O_{2-δ}, the reduction of Ni²⁺ species do not take place during reaction to metallic Ni species (see Fig. 3(b)) and higher OSC in comparison with Ce_{0.7}Cu_{0.1}Fe_{0.2}O_{2-δ} manifested the role of Ni in abstracting lattice O₂ from ceria. The reaction of H₂O with reduced Ce^{3+□} centers is suggested to release H₂, an increase in the number of reduced centers (in this case vacancies) would be directly related to OSC of catalyst and anticipated the improved activity. It is implicitly assumed in this model that the reaction takes place in adjacent metal cation and cerium active sites (interfacial area). It has been proposed that the dissociation of H₂O rather than CO adsorption is the rate limiting step [21,59]. Therefore, while deriving kinetic expression, it was explicitly assumed that dissociation of H₂O and CO₂ (i.e. oxidation of catalyst) is the rate limiting step. It seems that the ceria mediated processes of CO oxidation and WGS appeared to be controlled by two processes, namely, transfer of lattice or dissociated O₂ from ceria to the metal interface and re-oxidation of ceria [7].

To account for the reverse WGS reaction, the adsorption of H₂ over oxidized cation and CO₂ over oxide vacancy is proposed by equations (7) and (9), respectively. It has been well reported that the interplay between CO₂ and H₂O inhibits dissociative adsorption of H₂O [60]. So, we modeled this step as competitive adsorption between CO₂ and H₂O for same active sites. The interaction of CO₂ over oxide vacancy results in the oxidation of catalyst and release of CO molecule as represented by equation (10). The adsorbed H₂ species extracts lattice oxygen from ceria, giving out H₂O molecule along with reduction of catalyst (equation (8)). In this case, S becomes S* and this oxygen reacts with hydrogen to form water. This mechanism was proposed taking into consideration that there are two kind of active sites present on the catalyst surface. The balance on the active sites can be written as

$$[\text{S}] + [\text{S}^*] + [\text{CO} - \text{S}^*] + [\text{H}_2 - \text{S}^*] = 1 \quad (11)$$

$$[\text{Ce}^{4+}] + [\text{Ce}^{3+\square}] + [\text{H}_2\text{O} - \text{Ce}^{3+\square}] + [\text{CO}_2 - \text{Ce}^{3+\square}] = 1 \quad (12)$$

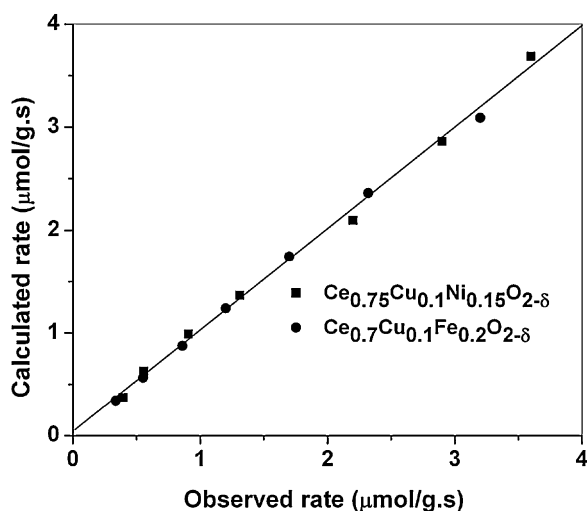


Fig. 10. Comparison between experimentally measured rate and calculated rate from the model.

The bracketed quantity in the above equations indicates the coverage of various species present on the catalyst surface. Based on the above proposed steps, the rate of reaction is given by

$$r_{\text{overall}} = \frac{(K_1 k_2 C_{\text{CO}} + K_6 k_7 C_{\text{H}_2}) (K_3 K_4 k_5 C_{\text{H}_2\text{O}} - K_8 k_{59} C_{\text{CO}_2})}{(K_1 C_{\text{CO}} + K_1 k_{25} C_{\text{CO}} + K_6 k_{57} C_{\text{H}_2}) + (K_3 C_{\text{H}_2\text{O}} + k_8 C_{\text{CO}_2}) (K_1 k_{25} C_{\text{CO}} + k_6 k_{57} C_{\text{H}_2})} \quad (13)$$

The limiting rate expression for forward WGS reaction is written as

$$r_{\text{forward}} = \frac{K_1 K_3 k_{25} k_4 C_{\text{CO}} C_{\text{H}_2\text{O}}}{1 + K_1 k_{25} C_{\text{CO}} + K_1 K_3 k_{25} C_{\text{CO}} C_{\text{H}_2\text{O}}} \quad (14)$$

Note that the notation k_{ij} in the equation (13) and (14) denotes a product of k_i and k_j (i.e. $k_{ij} = k_i \times k_j$). The parameters appearing in the rate equation (14) were estimated using a non-linear regression algorithm based on Levenberg-Marquardt technique. Because there are four parameters, appropriate constraints were imposed while optimizing rate parameters. The constraints were that the activation energies and the frequency factors have to be positive while the adsorption parameters were taken from the literature. The value of the equilibrium constants (K_1) for CO adsorption and dissociation of H_2O on the oxide (k_4), were taken from the literature [27,56] and used as initial guesses in the regression. Thus, optimized parameter K_3 and k_{25} were obtained for both catalysts. The sensitivity analysis was also performed by changing K_3 , k_{25} and K_1 parameters and the value of k_4 parameter was estimated. The results of regression indicate that the change in the value of K_3 , k_{25} and K_1 parameters do not have a significant effect on the predicted value and in each case the change in the value of k_4 parameter was small. Therefore, it was felt that K_1 , K_3 , k_{25} can be kept same and only k_4 need to be adjusted to fit the data. By comparing the rate constant values for the elementary steps, it can be concluded that dissociation of H_2O over oxide (step 5) is the slowest step in the mechanism. This is in agreement to the results reported in the literature. This mechanism indicates that the reducibility of the catalyst increases the WGS activity. Thus step 5, which represents dissociation of H_2O , is proportional to oxide vacancy. An increase in the reducibility of the catalyst leads to an increase oxide vacancy, and thus, as the catalyst reducibility increases, the rate of reaction also increases. By comparing the rate constants (k_4) for step 5 over both the catalysts from Table 4, it can be noted that the activation energies are nearly same for both the catalysts. However, the pre-exponential factor is higher for $\text{Ce}_{0.75}\text{Cu}_{0.1}\text{Ni}_{0.15}\text{O}_{2-\delta}$ catalyst compared to $\text{Ce}_{0.7}\text{Cu}_{0.1}\text{Fe}_{0.2}\text{O}_{2-\delta}$ catalyst indicating that the former catalyst is more reducible than the latter, which is

Table 4

Optimized rate parameters for WGS reaction over $\text{Ce}_{0.75}\text{Cu}_{0.1}\text{Ni}_{0.15}\text{O}_{2-\delta}$ and $\text{Ce}_{0.7}\text{Cu}_{0.1}\text{Fe}_{0.2}\text{O}_{2-\delta}$.

Parameter	$\text{Ce}_{0.75}\text{Cu}_{0.1}\text{Ni}_{0.15}\text{O}_{2-\delta}$	$\text{Ce}_{0.7}\text{Cu}_{0.1}\text{Fe}_{0.2}\text{O}_{2-\delta}$
K_1	$30 \times \sqrt{T} \exp(3001/T)$	$30 \times \sqrt{T} \exp(3001/T)$
K_3	$475 \times \sqrt{T}$	$475 \times \sqrt{T}$
k_4	$18 \times \exp(-5558/T)$	$11 \times \exp(-5783/T)$
k_{25}	$7 \times \exp(-1000/T)$	$7 \times \exp(-1000/T)$

consistent with our H_2 -TPR results. Based on these, the optimized rate parameters obtained from equation (14) are reported in Table 4 for $\text{Ce}_{0.75}\text{Cu}_{0.1}\text{Ni}_{0.15}\text{O}_{2-\delta}$ and $\text{Ce}_{0.7}\text{Cu}_{0.1}\text{Fe}_{0.2}\text{O}_{2-\delta}$ catalysts. Fig. 10 shows the predicted rate of reaction corresponding to the experimental observed reaction rate. It can also be observed from Fig. 10 that the model could describe the process reasonably well.

4. Conclusions

The activity of ceria for the water gas shift reaction was significantly enhanced due to the ionic substitution of base metals and this is attributed to the enhanced reducibility of ceria. The largest synergic interaction was displayed by the Cu-Ni-modified ceria catalyst. The relatively low activity exhibited by the Cu-Fe-modified ceria compared to Cu-Ni-modified ceria catalyst can be explained

by the fact that Fe metals are likely to be oxidized under reaction conditions and therefore unlikely to stabilize CO adsorption. The presence of excess water vapor suppressed the adsorption of CO_2 over these catalysts and the reverse WGS reaction. The surface structures of ceria modified compounds are highly reversible in cyclic redox conditions. Partial reoxidation of a catalyst reduced at 600°C occurs even at room temperature. Therefore, the studied catalysts are promising as new high oxygen storage materials and are highly competitive to noble metals. A mechanism involving a redox process, with oxidation of CO adsorbed on the metal cations by oxygen supplied to the metal interface by ceria, followed by H_2O replenishing of oxygen vacancy on ceria was proposed. The results of the present study are expected to be an important component for the development of potentially new cost effective catalysts for the water gas shift reaction.

Acknowledgment

The authors thank the Department of Science and Technology, India for financial support.

References

- [1] G. Jacobs, P.M. Patterson, L. Williams, E. Chenu, D. Sparks, G. Thomas, B.H. Davis, *Applied Catalysis A* 262 (2004) 177–187.
- [2] A. Faur Ghenciu, *Current Opinion in Solid State & Materials Science* 6 (2002) 389–399.
- [3] X. Wang, J.A. Rodriguez, J.C. Hanson, D. Gamarra, A. Martínez-Arias, M. Fernández-García, *Journal of Physical Chemistry B* 110 (2006) 428–434.
- [4] D.J. Suh, C. Kwak, J.H. Kim, S.M. Kwon, T.J. Park, *Journal of Power Sources* 142 (2005) 70–74.
- [5] R. Gorte, S. Zhao, *Catalysis Today* 104 (2005) 18–24.
- [6] W. Ruettinger, O. Ilinich, R.J. Farrauto, *Journal of Power Sources* 118 (2003) 61–65.
- [7] G. Jacobs, L. Williams, U. Graham, G.A. Thomas, D.E. Sparks, B.H. Davis, *Applied Catalysis A* 252 (2003) 107–118.
- [8] P.A. Deshpande, M.S. Hegde, G. Madras, *Applied Catalysis B* 96 (2010) 83–93.
- [9] Y. Li, Q. Fu, M. Flytzani-Stephanopoulos, *Applied Catalysis B* 27 (2000) 179–191.
- [10] N. Mahadevaiah, P. Singh, B.D. Mukri, S.K. Parida, M.S. Hegde, *Applied Catalysis B* 108–109 (2011) 117–226.

- [11] A. Luengnaruemitchai, S. Osuwan, E. Gulari, *Catalysis Communications* 4 (2003) 215–221.
- [12] F. Bocuzzi, A. Chiorino, M. Manzoli, D. Andreeva, T. Tabakova, *Journal of Catalysis* 188 (1999) 176–185.
- [13] M. Boaro, M. Vicario, J. Llorca, C. De Leitenburg, G. Dolcetti, A. Trovarelli, *Applied Catalysis B* 88 (2009) 272–282.
- [14] M. Haruta, *Catalysis Today* 36 (1997) 153–166.
- [15] D. Tibiletti, F. Meunier, A. Goguet, D. Reid, R. Burch, M. Boaro, M. Vicario, A. Trovarelli, *Journal of Catalysis* 244 (2006) 183–191.
- [16] E. Chenu, G. Jacobs, A.C. Crawford, R.A. Keogh, P.M. Patterson, D.E. Sparks, B.H. Davis, *Applied Catalysis B* 59 (2005) 45–56.
- [17] Y. Wang, S. Liang, A. Cao, R.L. Thompson, G. Vesper, *Applied Catalysis B* 99 (2010) 89–95.
- [18] P.S. Lambrou, C.N. Costa, S.Y. Christou, A.M. Efstathiou, *Applied Catalysis B* 54 (2004) 237–250.
- [19] S.Y. Christou, S.G. Rodríguez, J.L.G. Fierro, A.M. Efstathiou, *Applied Catalysis B* 111–112 (2012) 233–245.
- [20] D. Andreeva, V. Idakiev, T. Tabakova, L. Ilieva, P. Falaras, A. Bourlinos, A. Travlos, *Catalysis Today* 72 (2002) 51–57.
- [21] T. Bunluesin, R. Gorte, G. Graham, *Applied Catalysis B* 15 (1998) 107–114.
- [22] T. Shido, Y. Iwasawa, *Journal of Catalysis* 141 (1993) 71–81.
- [23] M. Sanchez, J. Gazquez, *Journal of Catalysis* 104 (1987) 120–135.
- [24] P. Fornasiero, R. Dimonte, G.R. Rao, J. Kaspar, S. Meriani, A. Trovarelli, M. Graziani, *Journal of Catalysis* 151 (1995) 168–177.
- [25] H. Yao, Y.F. Yao, *Journal of Catalysis* 86 (1984) 254–265.
- [26] K. Azzam, I. Babich, K. Seshan, L. Lefferts, *Journal of Catalysis* 251 (2007) 153–162.
- [27] A.A. Gokhale, J.A. Dumesic, M. Mavrikakis, *Journal of the American Chemical Society* 130 (2008) 1402–1414.
- [28] C.M. Kalamaras, I.D. Gonzalez, R.M. Navarro, J.L.G. Fierro, A.M. Efstathiou, *Journal of Physical Chemistry C* 115 (2011) 11595–11610.
- [29] N. Schumacher, A. Boisen, S. Dahl, A.A. Gokhale, S. Kandoi, L.C. Grabow, J.A. Dumesic, M. Mavrikakis, I. Chorkendorff, *Journal of Catalysis* 229 (2005) 265–275.
- [30] Q. Fu, W. Deng, H. Saltsburg, M. Flytzani-Stephanopoulos, *Applied Catalysis B* 56 (2005) 57–68.
- [31] P. Bera, K. Priolkar, P. Sarode, M.S. Hegde, S. Emura, R. Kumashiro, N. Lalla, *Chemistry of Materials* 14 (2002) 3591–3601.
- [32] A.P. Grosvenor, M.C. Biesinger, R.S.C. Smart, N.S. McIntyre, *Surface Science* 600 (2006) 1771–1779.
- [33] A.M. Visco, F. Neri, G. Neri, A. Donato, C. Milone, S. Galvagno, *Physical Chemistry Chemical Physics* 1 (1999) 2869–2873.
- [34] S. Minico, S. Scire, C. Crisafulli, A. Visco, S. Galvagno, *Catalysis Letters* 47 (1997) 273–276.
- [35] V. Schwartz, D.R. Mullins, W. Yan, B. Chen, S. Dai, S.H. Overbury, *Journal of Physical Chemistry B* 108 (2004) 15782–15790.
- [36] K.D. Jung, A.T. Bell, *Journal of Catalysis* 193 (2000) 207–223.
- [37] H. Sakurai, A. Ueda, T. Kobayashi, M. Haruta, *Chemical Communications* (1997) 271–272.
- [38] S. Hilaire, X. Wang, T. Luo, R. Gorte, J. Wagner, *Applied Catalysis A* 215 (2001) 271–278.
- [39] R. Leppelt, B. Schumacher, V. Plzak, M. Kinne, R. Behm, *Journal of Catalysis* 244 (2006) 137–152.
- [40] C. Rhodes, G. Hutchings, A. Ward, *Catalysis Today* 23 (1995) 43–58.
- [41] A.A.E. Moemen, G. Kučerová, R.J. Behm, *Applied Catalysis B* 95 (2010) 57–70.
- [42] G. Millar, C. Rochester, K. Waugh, *Journal of Catalysis* 142 (1993) 263–273.
- [43] T. Shido, Y. Iwasawa, *Journal of Catalysis* 129 (1991) 343–355.
- [44] C.M. Kalamaras, G.G. Olympiou, A.M. Efstathiou, *Catalysis Today* 138 (2008) 228–234.
- [45] G. Jacobs, L. Williams, U. Graham, D. Sparks, B.H. Davis, *Journal of Physical Chemistry B* 107 (2003) 10398–10404.
- [46] T. Van Herwijnen, R. Guzaliski, W. De Jong, *Journal of Catalysis* 63 (1980) 94–101.
- [47] C.M. Kalamaras, S. Americanou, A.M. Efstathiou, *Journal of Catalysis* 279 (2011) 287–300.
- [48] D. Tibiletti, A. Goguet, F.C. Meunier, J.P. Breen, R. Burch, *Chemical Communications* (2004) 1636–1637.
- [49] A. Goguet, F.C. Meunier, D. Tibiletti, J.P. Breen, R. Burch, *Journal of Physical Chemistry B* 108 (2004) 20240–20246.
- [50] D. Tibiletti, A. Goguet, D. Reid, F.C. Meunier, R. Burch, *Catalysis Today* 113 (2006) 94–101.
- [51] K. Azzam, I. Babich, K. Seshan, L. Lefferts, *Applied Catalysis B* 80 (2008) 129–140.
- [52] M. Tinkle, J. Dumesic, *Journal of Catalysis* 103 (1987) 65–78.
- [53] S. Hilaire, S. Sharma, R. Gorte, J. Vohs, H.W. Jen, *Catalysis Letters* 70 (2000) 131–135.
- [54] C.M. Kalamaras, P. Panagiotopoulou, D.I. Kondarides, A.M. Efstathiou, *Journal of Catalysis* 264 (2009) 117–129.
- [55] F. Meunier, D. Reid, A. Goguet, S. Shekhtman, C. Hardacre, R. Burch, W. Deng, M. Flytzani-Stephanopoulos, *Journal of Catalysis* 247 (2007) 277–287.
- [56] C.T. Campbell, K. Daube, *Journal of Catalysis* 104 (1987) 109–119.
- [57] C. Ovesen, P. Stoltze, J. Norskov, C. Campbell, *Journal of Catalysis* 134 (1992) 445–468.
- [58] J. Nakamura, J.M. Campbell, C.T. Campbell, *Journal of the Chemical Society, Faraday Transactions* 86 (1990) 2725–2733.
- [59] C.D. Zeinalipour-Yazdi, A.M. Efstathiou, *Journal of Physical Chemistry C* 112 (2008) 19030–19039.
- [60] R. Burch, *Physical Chemistry Chemical Physics* 8 (2006) 5483–5500.